Remotely Sensing Larval Population Dynamics of Rice Field Anophelines

Louisa R. Beck[1], Sheri W. Dister[2], Byron L. Wood[3], Robert K. Washino[4]

[1]California State University Monterey Bay, MS 242-4, NASA Ames Research Center, Moffett Field, CA 94035
[2]Johnson Controls, MS 242-4, NASA Ames Research Center, Moffett Field, CA 94035
[3]Ecosystem Science & Technology Branch, MS 242-4, NASA Ames Research Center, Moffett Field, CA 94035
[4]Department of Entomology, University of California, Davis, CA 95616

Introduction

Efficient and successful mosquito control is often dependent on the ability of agencies to identify larval habitat and then to distinguish between high- and low-producing habitats in a timely manner. Typically, ground survey techniques, which involve extensive field work and intensive manual labor, are impractical over large areas due to time and financial constraints. One approach to regional surveillance of larval habitats is to use remote sensing data to assess vegetation parameters associated with high larval-producing habitats. Early studies of mosquito habitats using remotely sensed data primarily focused on identifying and mapping aquatic environments to assess the spatial distribution of potential larval habitat (Barnes & Cibula, 1979; Hayes *et al.*, 1985; Welsh *et al.*, 1989). In 1985, the National Aeronautics and Space Administration (NASA) initiated a project called the Biospheric Monitoring and Disease Prediction Project (Di-Mod), whose goal was to determine if remotely sensed data could be used to identify and monitor environmental parameters that influence malaria vector populations, and therefore disease transmission risk (NASA, 1988).

Background

Remote sensing. All objects on the earth's surface transmit, reflect, and/or absorb electromagnetic (EM) energy from the sun, and each object does so differently depending on its physical properties. In the visible portion of the EM spectrum, where our eyes perceive objects, leaf pigments in a healthy green leaf absorb energy in the red wavelengths and reflect energy in the green; that's why plants appear to be green. Beyond the visible wavelengths, in the infrared portion of the spectrum, green leaves have a very characteristic reflectance response that we can't see. In the near-infrared, the internal structure of a plant's leaf results in very high reflectance of EM energy, and in the mid-infrared, the water content of a leaf affects its reflectance. A plant's spectral response in the visible, near-, and mid-infrared wavelengths of the EM spectrum, called its "spectral curve" (Figure 1), will depend on the type and condition of the plant itself, as well as the angle of the sun's rays hitting the object, atmospheric conditions, topographic position, and so forth.

The spectral curves of vegetation, and of other objects on the earth's surface, can be detected and measured using special instruments that have been designed to record reflectance in specific wavelengths. These instruments, called sensors, can function in wavelengths beyond those we can detect with our own eyes, enabling

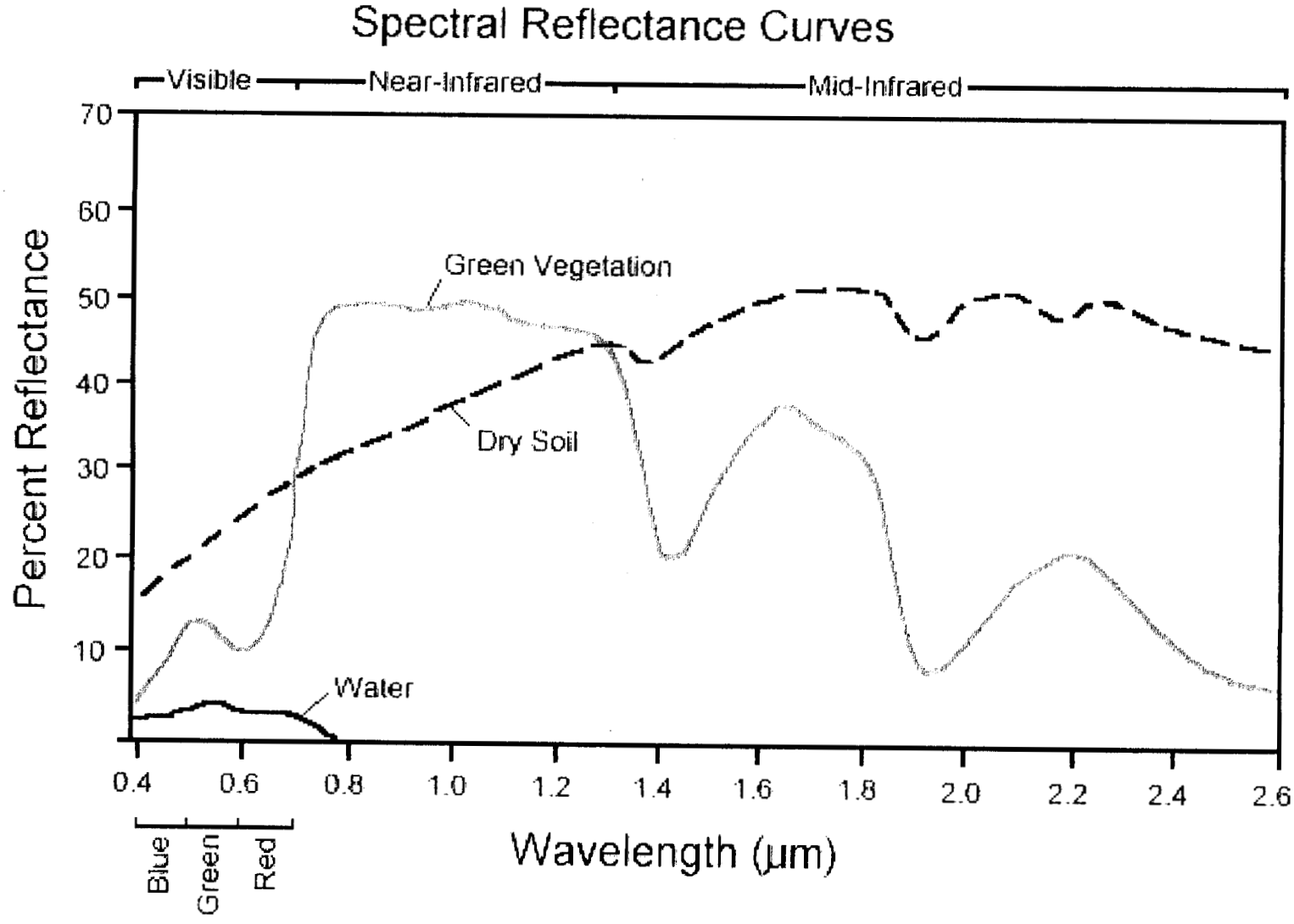
Spectral Reflectance Curves
Visible
Near-Infrared
Mid-Infrared
Percent Reflectance
70
60
50
40
30
20
10
Green Vegetation
Dry Soil
Water
0.4
0.6
0.8
1.0
1.2
1.4
1.6
1.8
2.0
2.2
2.4
2.6
Blue
Green
Red
Wavelength (µm)

us to "see" unique reflectance properties of plants and other objects. These unique properties help us to then distinguish objects that may look similar to our eyes, and to map the distribution of objects more accurately. For example, remote sensing was used during World War II to distinguish healthy, growing vegetation from vegetation that had been cut for camouflaging military targets. These cut branches still appeared to be green to the human eye, but, due to moisture stress and other leaf damage, the branches reflected EM energy very differently in the near-infrared portion of the spectrum. Special film that could record differences in near-infrared reflectance was developed and used to locate these targets based on their anomalous reflectance patterns. This phenomenon, called "pre-visual stress," is now exploited to map the distribution of diseased or stressed crops and forests whose damaged internal leaf structure has yet to affect their reflectance patterns in the visible wavelengths.

In figure 1, note how a healthy green leaf reflects energy in the green, absorbs in the red, and highly reflects in the near-infrared. When leaves senesce and die, this curve changes significantly: a dying leaf will reflect less energy in the green, more in the red (causing the leaf to look brown), and less in the near-infrared. Also shown in Figure 1 are typical reflectance curves for water, which absorbs energy in both the visible and near-infrared, and for dry soil, which reflects more energy than plants in the visible and less energy in the near-infrared. Because the soil is dry, it reflects more energy in the mid-infrared than moist, green leaves. These spectral curves represent average reflectance responses; the curves themselves depend on many physical factors. For example, reflectance from water will depend on the amount of sediment it contains, as well as its chemical content, its surface roughness, and its depth. Soil reflectance is affected by soil type, color, topographic position, and moisture content.

Vegetation reflectance is associated with such factors as species type, growth stage, plant condition (health), leaf water content, canopy structure, plant density, and leaf angle. Knowledge of how these and other variables affect vegetation reflectance has enabled RS technology to be used in agricultural applications to perform crop type classification, crop condition assessment, and crop yield estimation. For crop type classification, spectral response patterns and canopy texture are used to distinguish between such crops as corn, soybeans, small grains, etc., and to generate area inventories. To facilitate classification, analysts use crop calendars, which provide spectral information on the seasonal changes in a crop's reflectance pattern. Because of seasonal changes in reflectance, classification usually requires multiple dates of RS data. For crop condition assessment, the analyst utilizes pre-visual spectral responses (previously described) and visible reflectance to detect vegetation affected by disease, water stress, insect damage, differences in fertilizer application, etc. If the analyst knows the typical yield of a crop per unit area, this information can be used to estimate crop yield by multiplying the yield by the area under cultivation, as mapped using RS data.

As part of both crop type classification and crop condition assessment, analysts use RS data to estimate vegetation "greenness." This measurement is derived from the ratio between the crop's simultaneous spectral reflectance in the red and the near-infrared portions of the spectrum. Recall that healthy green leaves absorb energy in the red and highly reflect in the near-infrared (Figure 1). In general, the larger the difference between these two simultaneously measured spectral responses, the greener the plant. This chapter will discuss how vegetation greenness from RS data were used to assess rice development stage, an important variable for predicting anopheline larval abundance in California rice fields.

Remote sensing and Anopheles freeborni *larval habitat.* Most anopheline larval habitats are highly localized, and can occur where temperature, humidity, precipitation, elevation, vegetation, and water quality are suitable. In California, the western malaria mosquito, *Anopheles freeborni,* is unevenly distributed throughout a variety of wetlands, but is most commonly found in the nearly 240,000 hectares of irrigated rice grown in the Central Valley (Figure 2). The biology of this mosquito has been intensively studied (Markos, 1951; Markos and Sherman, 1957; Bailey and Gieke, 1968; Washino, 1980). These studies indicate that *An. freeborni* larval abundance may be influenced by several factors, including rice field location, density of the initial mosquito infestation, plant density, and plant growth rate. Of particular interest for mosquito control purposes is that these studies have also shown that not all rice fields produce large numbers of mosquitoes.

Remote sensing data have been used to measure green-leaf area of rice (Martin & Heilman, 1986) and to estimate rice yields (Patel *et al.*, 1991). Studies conducted in California have demonstrated that airborne and satellite multispectral data can be used to identify and monitor rice field vegetation development (Wall *et al.*, 1980; Hlavka and Sheffner, 1988). At the beginning of our experiments, it was known that the spatial and temporal dynamics of *An. freeborni* larval populations appeared to be related to rice field location and vegetation development characteristics, both of which could be monitored using RS data. What was not known was if RS data could be used to distinguish between high- and low-producing larval rice fields for the purpose of directing control measures. This question was the focus of two related experiments, which will now be discussed.

The Studies

Study 1. Both RS experiments were conducted in California's lower Sacramento Valley, and focused on a 90,000-ha area within the Sutter-Yuba Mosquito Abatement District (Figure 2). In the initial experiment (Washino *et al.*, 1987; 1988; Wood *et al.*, 1991a), which took place in 1985, 46 irrigated rice fields were selected for mosquito larval sampling. Fields were chosen from a pool of candidate fields for which access permission from landowners had been granted. Fields were then selected so that travel times could be minimized between sampling sites while still capturing differences in cultivation practices throughout the area. The location of

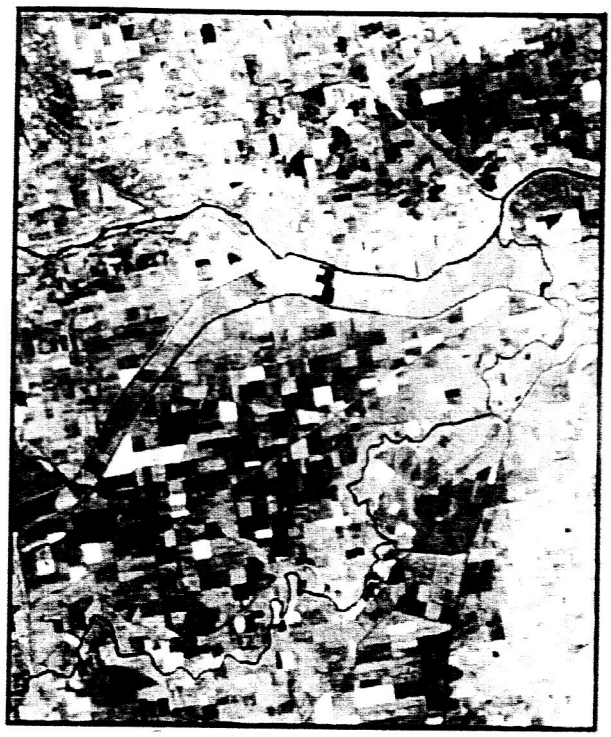

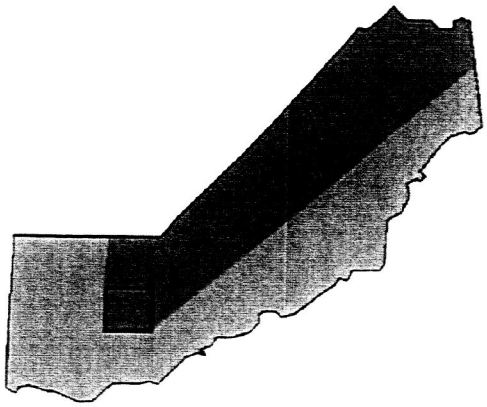

the fields to be sampled were plotted on 1:24,000-scale land-use maps produced by the California Department of Water Resources (DWR). Larval production in the lower Sacramento Valley usually begins in early July, and peaks in August; therefore, larval sampling was conducted at biweekly intervals between July and late August. The sampling protocol consisted of summing the number of *An. freeborni* larvae collected using 30 dips of a 500-ml dipping cup. Due to limited access allowed by land owners, these dips were taken randomly from a 2000-m^2 area along the edge of each rice field.

The remotely sensed data used in the experiment were acquired from both airborne and satellite platforms. Digital airborne Thematic Mapper Simulator (TMS) data, which "simulated" data from the Landsat Thematic Mapper (TM) instrument, were acquired throughout the growing season using a Daedalus multispectral scanner onboard NASA's ER-2 aircraft. This scanner recorded data in 12 wavebands, of which seven were identical to those of the Landsat TM sensor. Each picture element, or pixel, of data represented the spectral reflectance from a 28x28-m area on the ground. The first acquisition was on 11 June, and flights were conducted biweekly, coincident with larval sampling, until 16 October. Of the flights, seven were selected based on data quality: 11 June, 2 July, 23 July, 2 August, 27 August, 17 September, and 16 October. The TM-equivalent wavebands (with the exception of TMS-5 [the first mid-infrared channel] and TMS-6 [the thermal channel]) were extracted for each date. Data from bands 5 and 6 were omitted from further analysis due to poor data consistency from date to date. The five extracted bands were: TMS-1 (0.45–0.52 μm, blue), TMS-2 (0.52–0.60 μm, green), TMS-3 (0.63–0.69 μm, red), TMS-4 (0.76–0.90 μm, near-infrared), and TMS-7 (2.08–2.35 μm (second mid-infrared).

Figure 3 shows the position of the five extracted TMS bands with respect to a typical vegetation spectral curve for a green leaf. Within each bandwidth, all reflected energy was captured and averaged into a single digital number (DN), representing values between 0 and 255 (i.e., 8-bit data). Therefore, every 28x28-m pixel in an image contained five DNs, representing the simultaneous reflectance of that pixel in the blue, green, red, near-, and mid-infrared portions of the spectrum. Prior to the analysis, the spectral data were corrected for sun angle effects and each DN was converted to percent reflectance so that data acquired on different dates could be directly compared. Finally, mean reflectance values were extracted for each of the five wavebands using a 1x2-pixel polygon, which corresponded to the location of the sample plot within each rice field.

The larval sampling data collected throughout the season were used to estimate *An. freeborni* production for each field. Of the 46 fields sampled, seven accounted for over 50 percent of the seasonal production, and 24 fields produced over 90 percent. The seasonal production data were then used to divide the 46 fields into a "high" and a "low" larval-producing group. When these groups were plotted on the DWR land-use maps, it was revealed that the high larval-producing fields were clustered in a portion of the study area that contained a variety of land uses,

particularly livestock pastures. Using the DWR maps, it was determined that over 70 percent of the high fields were within 1.5 km of a livestock pasture, where adult *An. freeborni* could potentially find bloodmeal sources. Conversely, the majority of the low larval-producing fields were in areas devoted almost exclusively to rice, and were more than 1.5 km from the closest pasture.

To assess the utility of the TMS data for distinguishing between the high and low larval-producing fields, two statistical analyses were conducted. In one analysis, the TMS data were used to calculate a greenness value for each field. This was done using a variation of the greenness ratio discussed earlier. The greenness index, called the normalized difference vegetation index (NDVI), was calculated using the following formula:

$$(\text{TMS-4}_{\text{near-infraredDN}}) - \text{TMS-3}_{\text{redDN}}) \;/\; (\text{TMS-4}_{\text{near-infraredDN}}) + \text{TMS-3}_{\text{redDN}}).$$

The NDVI calculation was performed pixel-by-pixel on each of the seven dates, resulting in seven greenness values per pixel. The seven NDVI values for each 1x2-pixel site were averaged by group (high or low) and plotted by date in order to track the changes in greenness within a site throughout the sampling season. Although there was some spectral overlap between the high and low groups, 61.9 percent of the high larval-producing fields and 80.0 percent of the low-producing fields were spectrally separable on 11 June (Figure 4). By 2 July, when all rice fields were approaching full canopy development, the spectral overlap between high and low larval-producing fields had increased so that only 56.3 percent of the high fields and 20.0 percent of the low fields were separable. After 2 July, all rice fields were spectrally similar. This analysis indicated that NDVI values could be used to distinguish between high and low groups only early in the season, when rice fields were developing tillers and had yet to develop full canopies. This maximum difference was in June, nearly two months prior to the peak anopheline larval production.

A second statistical analysis was conducted in which the raw data (i.e., not the derived NDVI values) from the five TMS bands were used in a discriminant analysis (Davis, 1973; Swain and Davis, 1978). This procedure finds a linear combination of independent input variables that maximizes the difference between two previously defined groups. The resulting transformation is then used to separate the two groups and to determine how well the variables could identify group category for the observations. The five reflectance values, one for each of the five TMS wavebands, were used as the independent input variables to predict whether a plot belonged in the high or low larval-producing group; this was calculated for each of the seven dates. The results of the discriminant analysis showed that the TMS data could be used to distinguish between the high and low fields on both the 11 June and 2 July dates with greater than 75.0 percent accuracy, and that accuracies declined on the remaining dates. This result supports the findings of the NDVI analysis described above, in which NDVI values could separate high and low larval-producing fields with 80.0 percent accuracy.

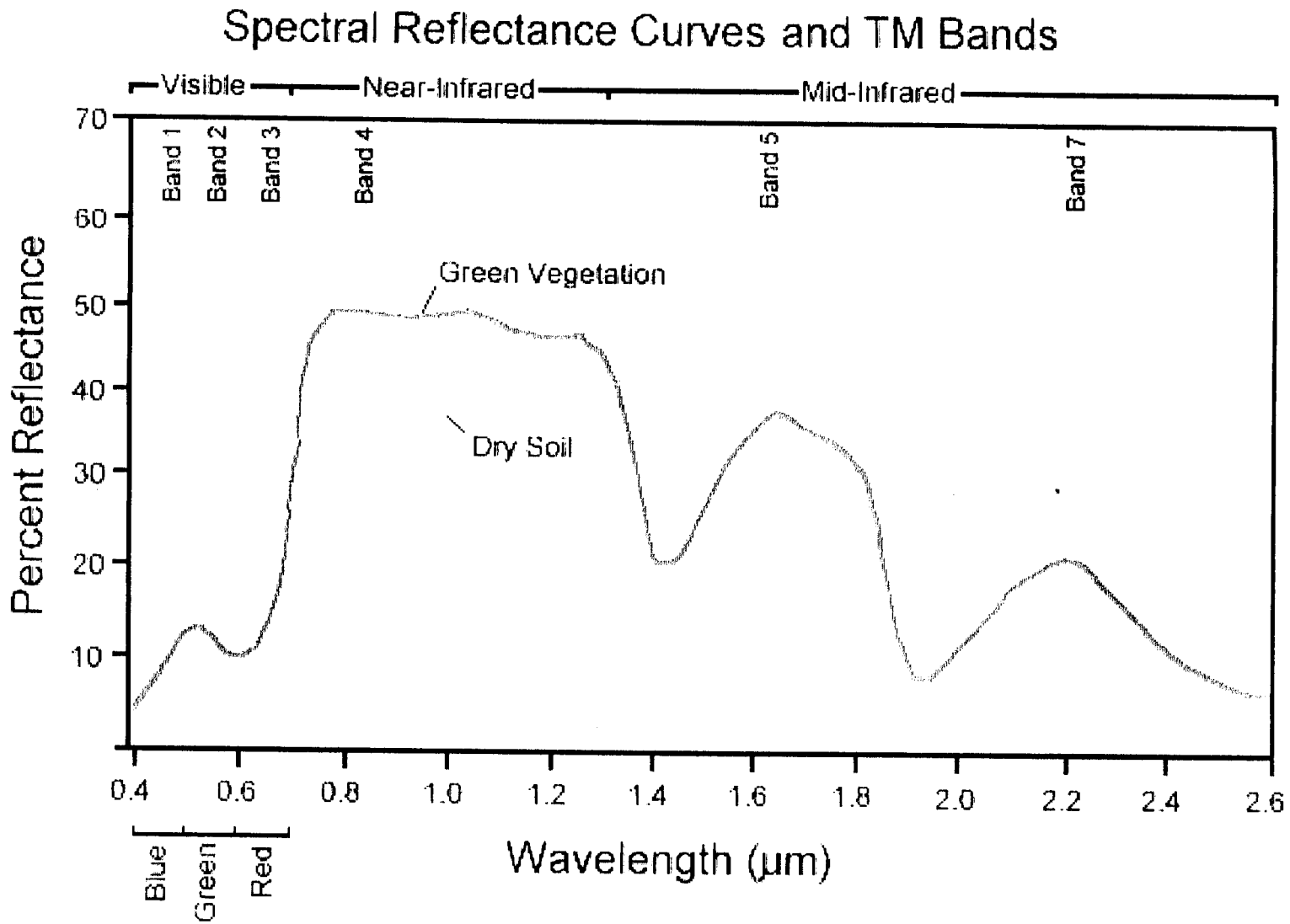
Spectral Reflectance Curves and TM Bands
Visible
Near-Infrared
Mid-Infrared
Band 1
Band 2
Band 3
Band 4
Band 5
Band 7
Green Vegetation
Dry Soil
Percent Reflectance
70
60
50
40
30
20
10
0.4
0.6
0.8
1.0
1.2
1.4
1.6
1.8
2.0
2.2
2.4
2.6
Blue
Green
Red
Wavelength (μm)

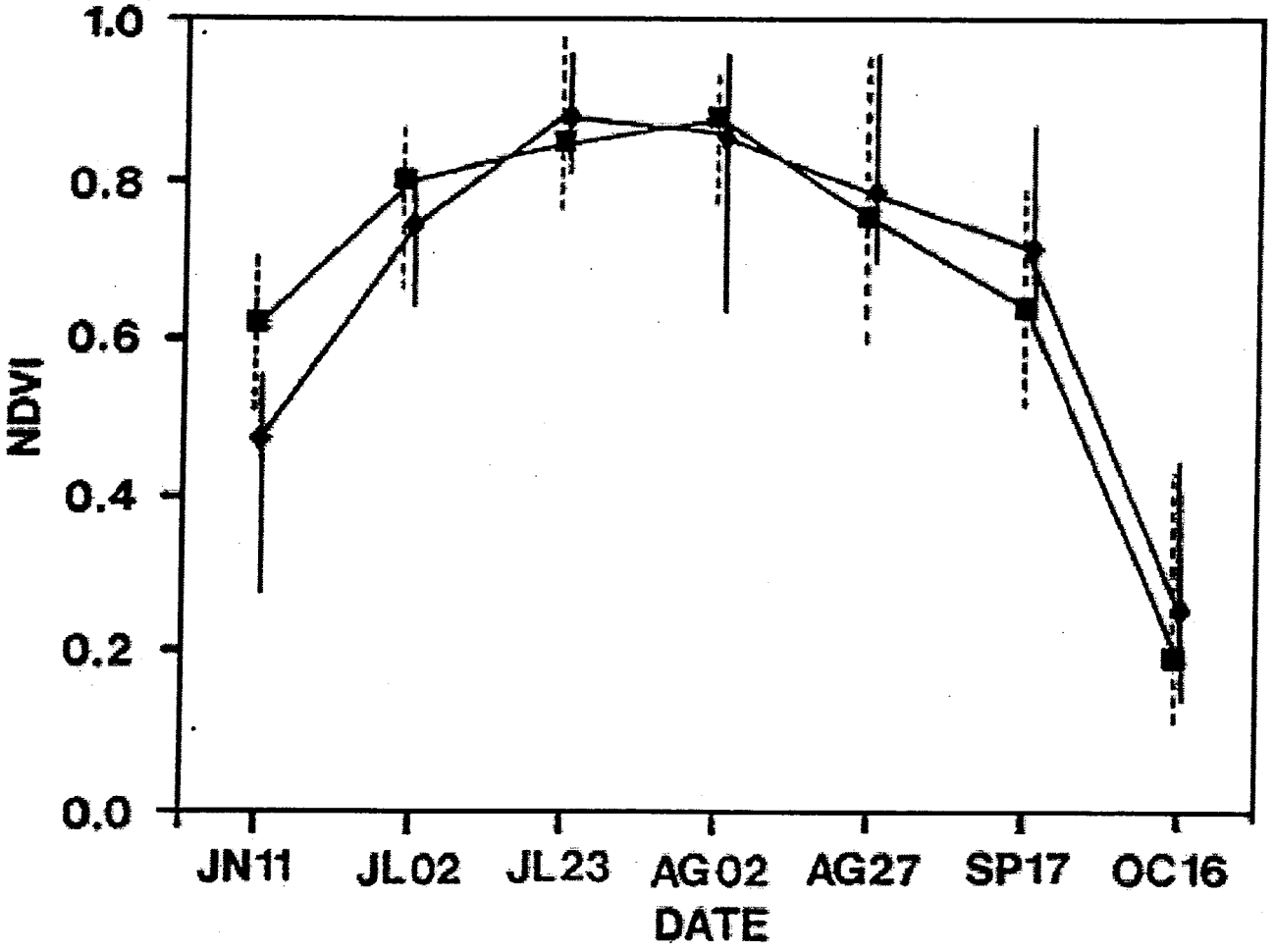
1.0
0.8
0.6
0.4
0.2
0.0
NDVI
JN11
JL02
JL23
AG02
AG27
SP17
OC16
DATE

Study 2. The outcome of the 1985 experiment suggested that rice fields that developed vegetative canopies earlier in the growing season, and that were located near livestock pastures, produced higher numbers of *An. freeborni* larvae than other rice fields. To test this hypothesis, another experiment was designed and conducted in the Sutter-Yuba Mosquito Abatement District in 1987 (Wood *et al.*, 1991b; 1992). The objectives of the new experiment were to (1) compare early-season spectral differences in canopy development of high and low larval-producing rice fields, (2) further explore the relationship between larval production in rice fields and the distance to a livestock pasture, and (3) determine if integrating the spectral and spatial (distance to pasture) measures could enhance the separation between high and low larval-producing fields. Additional analyses were later conducted to investigate how mosquito production and land cover surrounding a rice field were related. Results of this landscape analysis will also be reported.

A total of 104 irrigated rice fields were selected for intensive field sampling and spectral analysis. As in the earlier experiment, field selection was based on access (i.e., permission given by farmers to enter fields), and designed to minimize travel time between sites while maintaining variation in cultivation practices. Rectangular sampling plots, measuring approximately 2000 m^2, were established in each of the fields. Larval sampling was conducted on a weekly basis beginning on 29 June and continuing through to 3 September (i.e., 10 weeks). *An. freeborni* larvae abundance was assessed using 90 dips per field using a 500-ml dipping cup. Field crews also estimated percent canopy coverage within the sampling plots on a weekly basis, coincident with larval dipping, for the period between 18 May and 9 July. In August, when maximum canopy development was achieved, the field crews collected rice plants from five 0.1-m^2 plots in each field to determine rice tiller density and green-leaf area.

Several types of remotely sensed data were acquired over the study area during the experiment. These included airborne TMS data (described above), Landsat TM data, and airborne color-infrared photography. Table 1 lists the RS data acquisitions by date and sensor type. The spectral analyses were conducted on the same five TM or TM-equivalent bands used in the first experiment. The data were preprocessed prior to statistical analysis; this involved correcting the data for sun angle differences, and then converting the DNs to percent reflectance so that data from different sensors and dates could be directly compared. Following this correction, all data were geo-registered to a Universal Transverse Mercator (UTM) map projection so that the same pixels could be located on all dates. Once the data were registered, reflectances from each of the five channels were extracted from a 1x2-pixel area corresponding to the larval sampling locations in each field; this procedure was repeated for all 10 dates.

A digital land-use map was created from existing 1:24,000-scale DWR land-use maps. Because these DWR maps had been generated in 1984, the color-infrared photography (flown in May by NASA aircraft at a scale of 1:48,000) was used to

Table 1. Digital remote sensing data acquired over the study area in 1987. NS-001 and Daedalus are two types of airborne Thematic Mapper Simulator (TMS) data, designed to simulate Landsat Thematic Mapper (TM) data. Asterisks indicate the dates used in the spectral analyses.

Date	Sensor
20 May	NS-001 TMS
27 May*	Landsat-5 TM
19 June*	Daedalus TMS
28 June*	Landsat-5 TM
14 July	Landsat-5 TM
28 July	Daedalus TMS
6 August	Daedalus TMS

update the map. The location of the 104 rice fields were then plotted on the revised land-use map, enabling analysts to calculate distances between each rice field and the nearest livestock pasture (D). To calculate D, the minimum distance from the center of each of the 104 fields to the nearest livestock was measured, in kilometers, using the land-use map and geographic information system (GIS) functions. Two distance intervals were established, and the number of high and low larval-producing fields occurring within both intervals calculated. These intervals were 0–3 km and >3 km. The 3-km threshold was based on Bailey and Baerg (1967), whose work suggested that there is little dispersal of *An. freeborni* adults beyond the primary breeding areas during the summer months, even though this species' flight habits vary considerable throughout the year. When ranked in ascending order, there was a rapid decrease in the number of high larval-producing fields occurring beyond 3.0 km.

The seasonal larval production for each of the 104 fields was calculated by summing the number of *An. freeborni* larvae collected in each plot over the 10-week sampling period. The fields were then ranked in ascending order by larval count, and divided into a high or low group using 0.1 larva/dip as the threshold; this threshold was established by California mosquito abatement districts to distinguish high larval-producing fields and directing control measures (Figure 5). Using this threshold, it was found that approximately half of the 104 fields exceeded this value; therefore, for the analysis, fields were divided into two groups: 52 "high" and 52 "low" larval-producing fields. The larval density of each group was compared with measures of rice-tiller density, green-leaf area, and percent cover in order to determine if these field-measured parameters correlated with seasonal larval production. The field data were also used in the following statistical analyses to investigate the relationship between the vegetation measurements and the spectral data.

Analysis of the dipping data showed that seasonal larval production was dominated by only a small number of fields. Of the 104 fields sampled, 16 fields accounted for 50 percent, 36 fields accounted for 75 percent, and 52 fields accounted for 86 percent of the total seasonal production. This result was consistent with previous work by Washino (1980), as well as with the 1985 field data. As in the earlier experiment, the field data showed that the high-producing fields were grouped in areas in which livestock pastures were also found.

Regression analysis of the vegetation and larval data indicated that rice plant tiller density was positively correlated with larval production at the $p = 0.05$ level ($r = 0.21$) (Washino *et al.*, 1988). The other vegetation parameters were not correlated with larval abundance. The diagram shown in Figure 6, based on actual field measurements, illustrates the relationships between larval abundance, tiller density, and green-leaf area. These relationships suggest that fields with higher plant density and green-leaf area provide more favorable habitat for larval production.

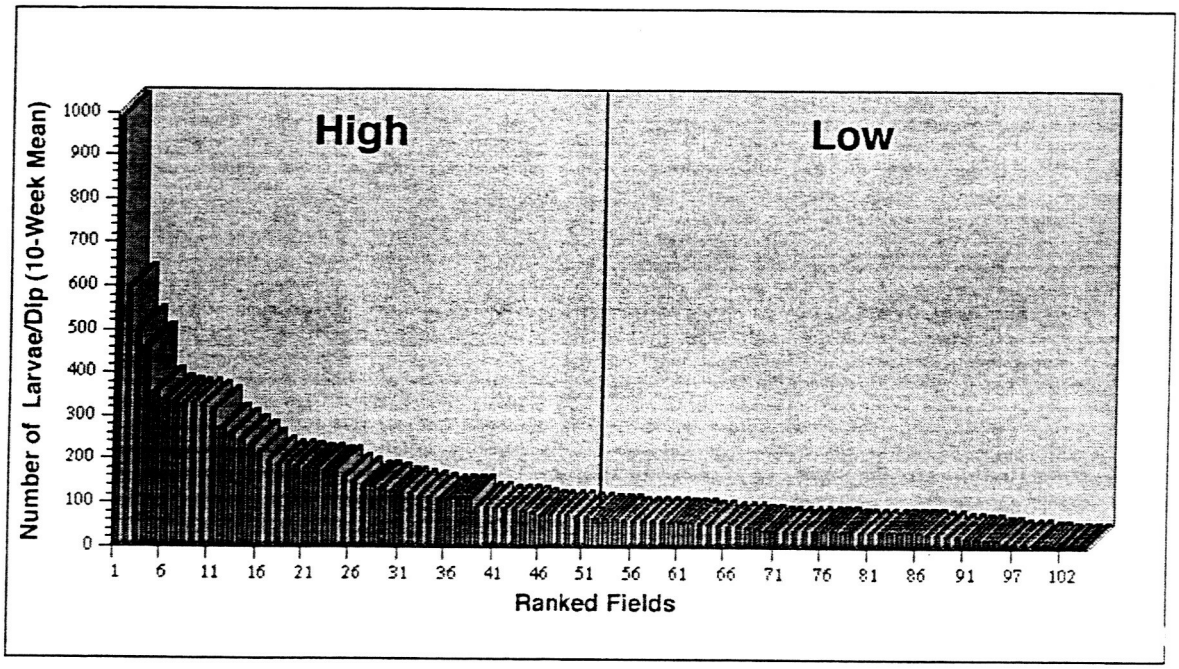
High
Low
Number of Larvae/Dip (10-Week Mean)
1000
900
800
700
600
500
400
300
200
100
0
1
6
11
16
21
26
31
36
41
46
51
56
61
66
71
76
81
86
91
97
102
Ranked Fields

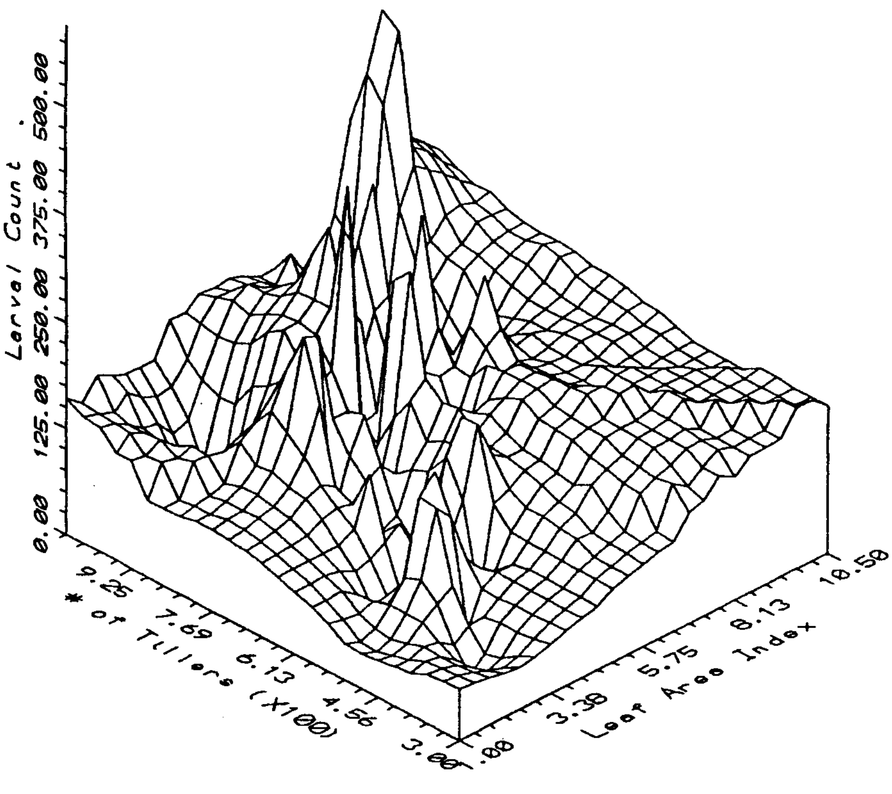

Larval Count
0.00
125.00
250.00
375.00
500.00
9.25
7.69
6.13
4.56
3.00
# of Tillers (X100)
.00
3.38
5.75
8.13
10.50
Leaf Area Index

Three separate of multivariate tests were conducted using different combinations of the spectral data and the distance-pasture measurements to determine how well these variables could distinguish between high and low larval-producing groups: (1) discriminant analysis of high and low groups, using only the spectral reflectance data; (2) discriminant analysis, using both the spectral data and distance-to-pasture measurements; and (3) a Bayesian approach that used *a priori* probabilities based on the distance-to-pasture measures to weight the spectral probabilities. A preliminary analysis, using mean NDVI values derived from the high and low larval-producing fields, showed that vegetation green-up in 1987 followed the same trend seen in the 1985 experiment (i.e., that the early season dates provided the best opportunity for spectral separation of the high and low groups). Therefore, the discriminant and Bayesian analyses were performed only on the three early-season dates: 27 May, 19 June, and 28 June.

Discriminant analysis using spectral data. This procedure was used in the 1985 experiment to determine which TM-equivalent bands, if any, could be used in a discriminant function to predict group membership (i.e., high versus low larval-producing). For each 1x2-pixel plot, the five DN values, representing the reflectances in the five TM wavebands for a field, were used as the independent input variables (*RS*) in a discriminant analysis to predict membership in the high (*H*) or low (*L*) larval-producing group. The output score, which was the likelihood of a field belonging to either the high ($P[H \mid RS]$) or the low ($P[L \mid RS]$) group was then used to categorize all 104 fields.

Discriminant analysis using spectral and distance data. For this analysis, the distance between each of the rice fields and the nearest livestock pasture (*D*) was used as an independent input variable, along with *RS*. The six input variables (five *RS* measurements plus *D*) determined the discriminant score, which was then used to categorize all 104 fields into either a high or low category.

Bayesian analysis using both spectral and distance measures. The third analysis used a Bayesian approach to distinguish high and low fields. Bayesian methods have been used by other investigators for combining data from diverse sources (e.g., spectral reflectance and topography) (Swain *et al.*, 1985; Strahler, 1980; Hutchinson, 1982). In this approach, prior probabilities based on the two distance measures ($P \mid D$) were used to weight probabilities based on RS data. Inside each distance interval, the conditional probability of a field belonging to either the high (*H*) or the low (*L*) group was estimated by dividing the probability of a field being high or low within a given interval by the probability of a field being within that distance interval. Table 2 shows the conditional probabilities of fields being high ($P[H \mid D]$) or low ($P[L \mid D]$) within each distance interval.

Three separate steps were taken in the Bayesian approach. The probability of a field being in the high or low group was estimated first based on *RS*; this resulted in two sets of probabilities: $P(H \mid RS)$ and $P(L \mid RS)$. Next, the probabilities from the first step were multiplied by the probabilities of each field being in the high or low

Table 2. Distance-to-pasture measurements (D) and conditional probabilities (P) of fields within each range belonging to the high [H] or low [L] larval-producing group based on distance alone.

	Distance (km)	
Group	0.0-2.9	3.0 +
No. High	44	9
No. Low	20	31
Probability		
$P[H]$	0.69	0.20
$P[L]$	0.31	0.80

group based on *D* (i.e., *P*[*H* | *D*]; *P*[*L* | *D*]). Finally, each field was assigned to the group that had the highest Bayesian score (*BAYES*).

Accuracy assessment. The classification accuracies for predicting the high group using the spectral data (*RS*) alone in a discriminant analysis were 63, 69, and 69 percent on 27 May, 19 June, and 28 June, respectively. Accuracies for the low group were 67, 56, and 65 percent, on the same dates. (All results are presented in Table 3.) By adding the sixth variable (*D*) in the second discriminant analysis method, the jackknifed classification accuracies for the high group rose to 75, 90, and 75 percent on 27 May, 19 June, and 28 June, respectively. Accuracies for the low group were roughly the same as those from the analysis using only *RS*: 64, 60, and 67 percent. Finally, the Bayesian approach for the three early season dates resulted in classification accuracies of 81, 85, and 75 percent for the high fields, and 67, 67, and 69 percent for the low fields.

Landscape composition analysis. The analyses involving *D*, the distance-to-pasture variable, indicated that the presence of land cover types other than rice influenced larval production. Therefore, an additional analysis, using geographic information system (GIS) techniques, was conducted to quantify, for each of the 104 rice fields, surrounding land uses, and then compare high and low larval-producing fields. The first step was to generate polygons of varying radii surrounding each rice field. These polygons, called "buffers," were created for distances of 1.0, 1.5, 2.0, 2.5, and 3.0 km from the edge of each field. These buffers were then used to summarize land cover information within that distance radius around each field. To do this, the buffers were overlain on the DWR land use map; then, for each rice field, the proportion of each land use type within each of the five distances was calculated. The land use categories included rice, field crops, occupied pasture (i.e., livestock present), unoccupied pasture, native vegetation, urban areas, and water (Figure 7).

Visual inspection showed that high larval-producing fields had greater heterogeneity in terms of surrounding land use; this relationship was particularly evident at the larger buffer distances. Low larval-producing rice fields tended to be surrounded by more rice fields and field crops. Correlation matrices of the land use proportions and the larval abundance data were generated to quantify these associations. High positive correlations with larval production were identified for pasture, orchard, and native vegetation (Figure 8). These three landscape elements provide opportunities for the mosquito to acquire a bloodmeal (such as from cows in pastures and small mammals in native vegetation), or to find a resting site (in shady orchards or native vegetation). The strongest associations were shown for the 2.5-km buffer. The area within this distance buffer incorporated a diversity of important cover types that were also within the flight range of *An. freeborni*. As expected, negative correlations were seen between larval abundance and the proportion of rice crops (i.e., the more rice and field crops surrounding a rice field, the fewer opportunities for bloodmeals and resting sites, and the less likely that the rice field will be used for egg-laying).

Table 3. Percentage correct identification by high and low group, based on discriminant analysis using only spectral data (*RS*), the spectral and distance measures (*RSD*), and using the Bayesian method (*BAYES*) for 27 May, 19 June, and 28 June.

	27 May			19 June			28 June		
Group	RS	RSD	BAYES	RS	RSD	BAYES	RS	RSD	BAYES
High	63	75	81	69	90	85	69	75	75
Low	67	64	67	56	60	67	65	67	69

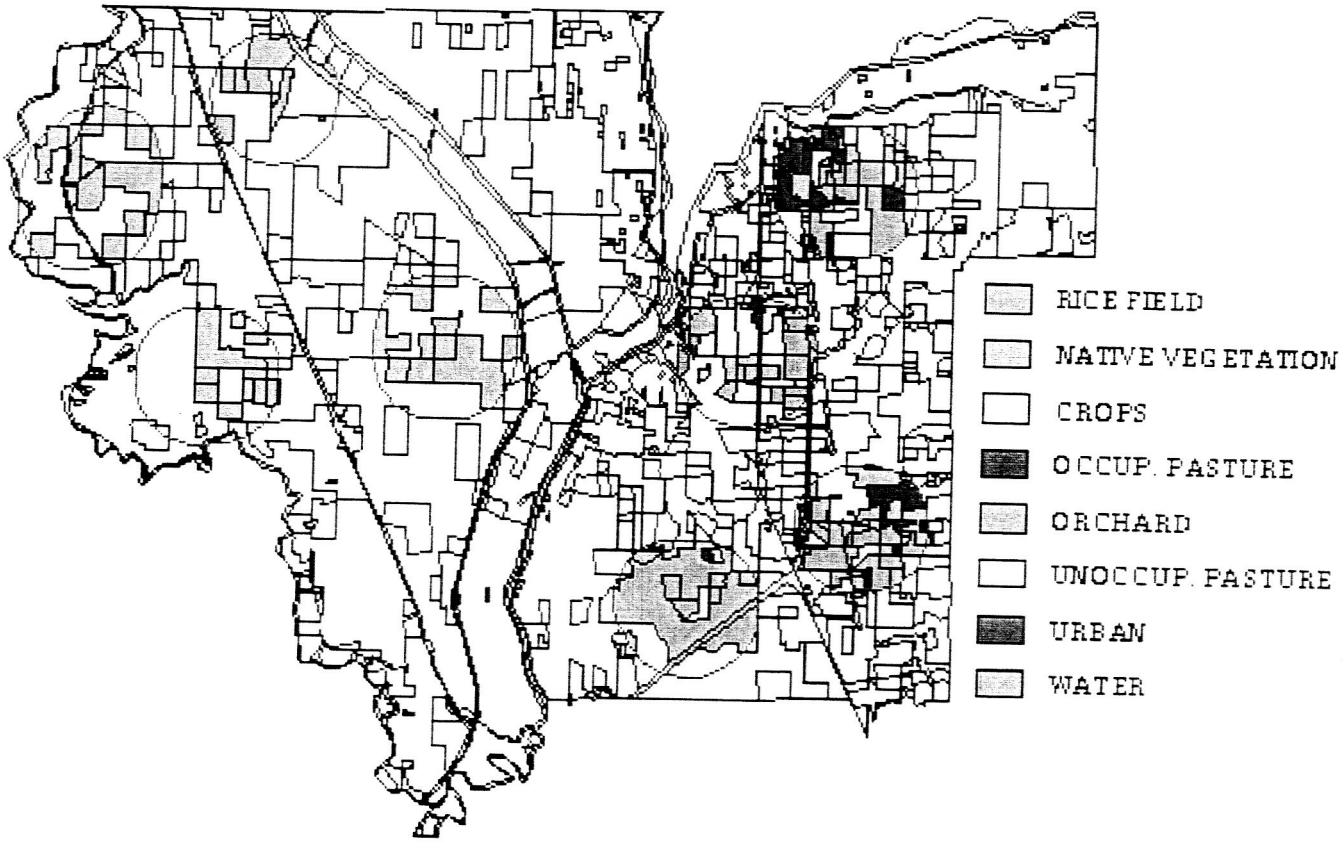
RICE FIELD
NATIVE VEGETATION
CROPS
OCCUP. PASTURE
ORCHARD
UNOCCUP. PASTURE
URBAN
WATER

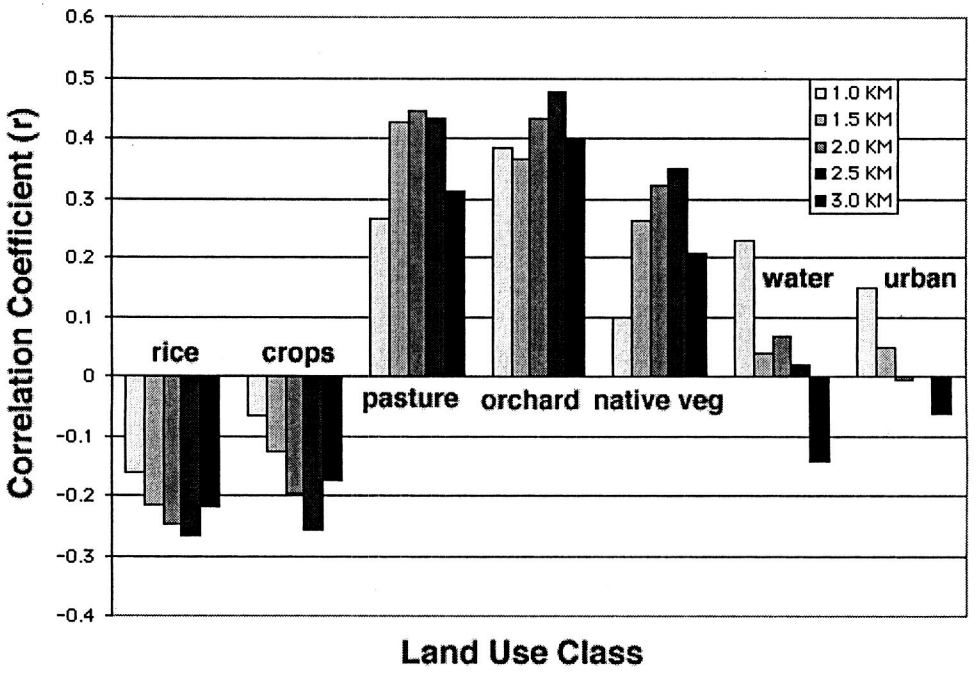
0.6
0.5
0.4
0.3
0.2
0.1
0
-0.1
-0.2
-0.3
-0.4
Correlation Coefficient (r)
1.0 KM
1.5 KM
2.0 KM
2.5 KM
3.0 KM
rice
crops
pasture
orchard
native veg
water
urban
Land Use Class

Discussion

The primary objective of both studies was to determine if RS and GIS techniques could be used to distinguish between high and low larval-producing rice fields in California. Results of the first study suggested that early-season green-up and proximity to livestock pastures were positively correlated with high larval abundance (Washino *et al.*, 1987; 1988; Wood *et al.*, 1991a). Based on the early-season spectral differences between high and low larval-producing fields, it appeared that canopy development and tillering influenced mosquito habitat quality. At that time, rice fields consisted of a mixture of plants and water, a combination that allowed *An. freeborni* females to lay eggs in partial sunlight, protected from both predators and wind. This established a population earlier in the season than in other, "less-green" fields where tillering and plant emergence was too minimal for ovipositioning. The study also indicated the importance of the distance that a mosquito would have to fly in order to take a bloodmeal prior to ovipositing. These associations were fully explored in an expanded study two years later. The second study confirmed the positive relationship between early season canopy development and larval abundance, and also demonstrated the relationship between abundance and distance-to-pasture. Figure 9 illustrates the association between greenness (as measured using NDVI), distance-to-pasture, and abundance. The second study also indicated the siginificance of the landscape context of rice fields for larval production. Fields that included opportunities for feeding and resting within the flight range of the mosquito had higher abundances than did fields that were in a homogeneous rice area.

Conclusion

Irrigated rice cultivation throughout the world constitutes one of the most important sources of anopheline larval habitats. In malaria-endemic areas of Asia, Africa, and the Americas, over 75 million hectares are devoted to irrigated rice. The spatial and temporal relationships between irrigated rice cultivation and *An. freeborni* population dynamics in California allowed investigators to use RS to characterize this association. The results indicated that RS data can be used to characterize early-season rice canopy development, which is a function of tillering and green-leaf area; these parameters can influence the quality of anopheline larval habitat. Combining the RS (spectral) and distance-to-pasture (spatial) information can enhance the identification of high larval-producing fields for use in directing early-season larval control measures. The methods described in this chapter could also be pertinent in other areas where irrigated rice is grown, with modifications for local differences in rice cultivars, cultivation practices, bloodmeal preferences, and larval habitat requirements.

The studies presented in this chapter used Landsat TM data or airborne TMS data. However, there are currently several RS sensors whose data could also be used for monitoring rice-field greenness on a local scale; these, and other sensors due to be launched onboard satellites in the next few years, are listed in Table 4. These

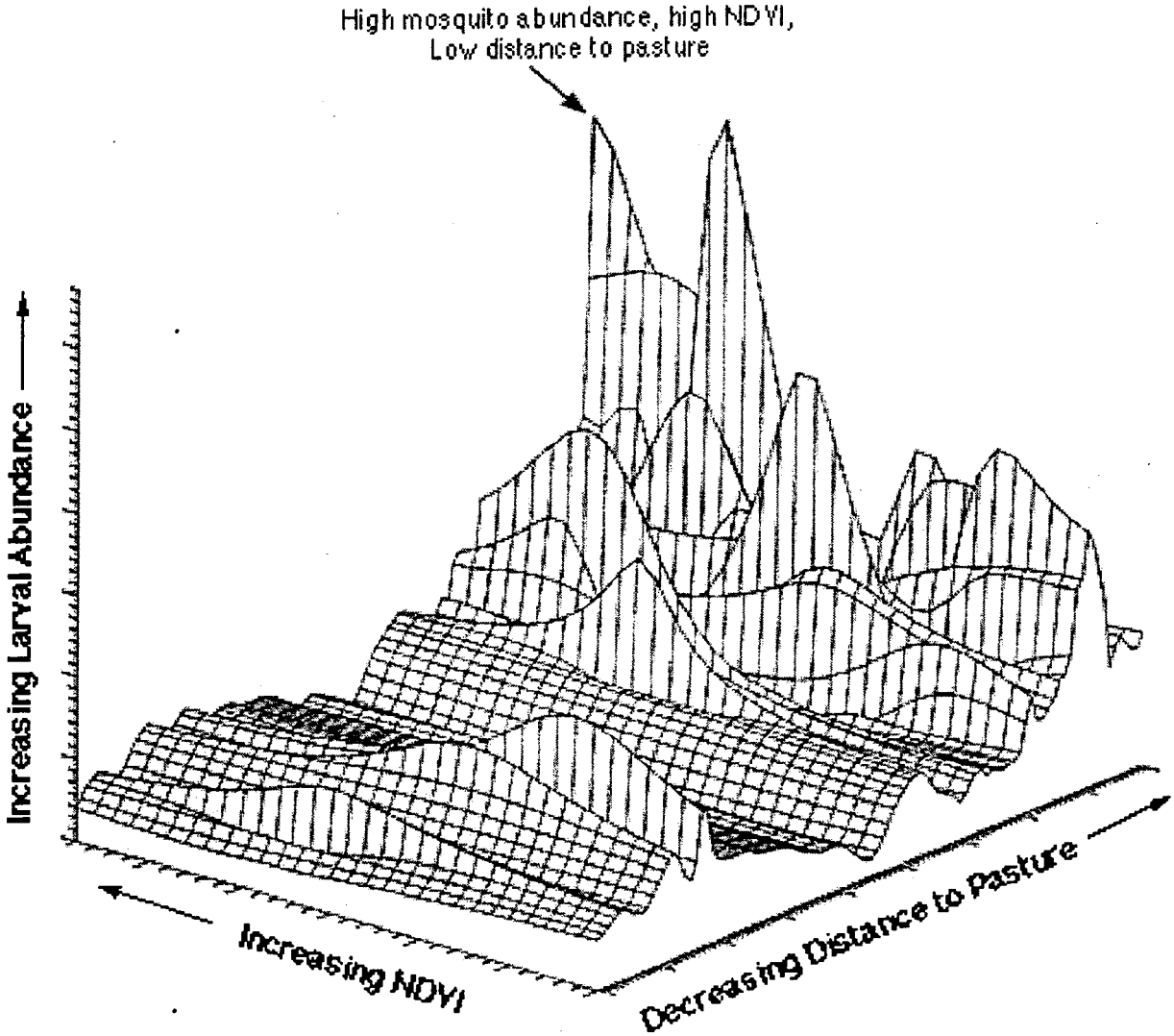
High mosquito abundance, high NDVI,
Low distance to pasture
Increasing Larval Abundance
Increasing NDVI
Decreasing Distance to Pasture

MISSION	COUNTRY	YEAR[1]	INSTRUMENT	RESOLUTION (m)	SWATH (km) [2]/ REPEAT (day)[3]
Landsat 5	USA	1984–	TM	30	185/16
IRS-1A	India	1988–	LISS II	36	148/22
SPOT-2	France	1990–	2xHRV	20	60/1-26
IRS-1B	India	1991–	LISS II	36	148/22
JERS-1	Japan	1992–	OPS	18	75/44
IRS P2	India	1994–	LISS II	36	132/24
IRS-1C	India	1995–	LISS III	23	142-148/24
Priroda/Mir	CIS[4]	1996–	MOMS-2P	6	44-88/14
IRS-1D	India	1997–	LISS III	23	142-148/24
SPOT-4	France	1998–	2xHRVIR	10, 20	60/3
Almaz-1b	CIS	(1998)	MSU-E2	10	2x24/3
Ikonos-1	SIE[5]	(1998)	MS	4	11x100/11
Ikonos-2	SIE	(1998)	MS	4	11x100/11
EOS-AM 1	USA/Japan	(1999)	ASTER	20	60/16
Landsat 7	USA	(1999)	ETM+	30	185/16
OrbView-3	Orbimage	(1999)	MS	4	8/3
QuickBird	USA	(1999)	QuickBird	3	22/1-4
ARIES-1	Australia	(2000)	ARIES	30	15/7
OrbView-4	Orbimage	(2000)	MS	4	5-8/3
ALOS	Japan	(2002)	AVNIR-2	10-15	35,70/2,45
SPOT-5a	France	(2002)	3xHRG	10	60/3
SPOT-5b	France	(2004)	3xHRG	10	60/3

1 Years followed by a hyphen indicate that the instruments are still acquiring data at the time of this writing; parenthetical dates are proposed launches

2 Area covered by the sensor

3 Days for satellite to pass over same place on the ground

4 Commonwealth of Independent States (former Soviet Union)

5 SpaceImaging EOSAT, Corp.

sensors are all capable of detecting spectral reflectance in the red and near-infrared portions of the spectrum, enabling users to generate NDVI values, and have spatial resolutions (i.e., less than 40x40 m) sufficiently fine to monitor rice field greenness.

The RS and GIS technologies have since been used to investigate the distribution of other disease vectors. Some of the studies supported by NASA include: *An. albimanus*, the vector of malaria in Chiapas, Mexico (Beck *et al.*, 1994; 1997); *Ixodes scapularis*, the vector of Lyme disease in the United States (Dister *et al.*, 1993; 1997); and *Culex pipiens*, the vector of filariasis in the Nile Delta (Hassan *et al.*, 1998a, b). For a more comprehensive discussion of RS/GIS and human health, the reader is referred to Hay *et al.*, 1996; 1997.

REFERENCES

Bailey, S., and D. Baerg. 1967. The flight habits of *Anopheles freeborni* Aitken. *Proc. 35th Ann. Conf. Calif. Mosq. and Vector Cont. Assoc.* Sacramento, CA, pp. 55–69.

Bailey, S.F., and P.A. Gieke. 1968. A study of the effect of water temperatures on rice field mosquito development. *Proc. Calif. Mosq. Control Assoc.* **36**:53–56.

Barnes, C., and W. Cibula. 1979. Some implications of remote sensing technology in insect control programs, including mosquitoes. *Mosq. News* **39**:271–282.

Beck, L.R., M.H. Rodríguez, S.W. Dister, A.D. Rodríguez, E. Rejmánková, A. Ulloa, R.A. Meza, D.R. Roberts, J.F. Paris, M.A. Spanner, R.K. Washino, C. Hacker, and L.J. Legters. 1994. Remote sensing as a landscape epidemiologic tool to identify villages at high risk for malaria transmission. *Am. J. Trop. Med. Hyg.* **51**:271–280.

Beck, L.R., M.H. Rodríguez, S.W. Dister, A.D. Rodríguez, R.K. Washino, D.R. Roberts, and M.A. Spanner. 1997. Assessment of a remote sensing based model for predicting malaria transmission risk in villages of Chiapas, Mexico. *Am. J. Trop. Med. Hyg.* **56**(1):99–106.

Dister, S.W., L.R. Beck, B.L. Wood, R. Falco, and D. Fish. 1993. The use of GIS and remote sensing technologies in a landscape approach to the study of Lyme disease transmission risk. *Proc.*, GIS '93: Geographic Information Systems in Forestry, Environmental and Natural Resource Management. Vancouver, B.C., Canada, 15–18 February 1993.

Dister, S.W., D. Fish, S. Bros, D.H. Frank, and B.L. Wood. 1997. Landscape characterization of peridomestic risk for Lyme disease using satellite imagery. *Am. J. Trop. Med. Hyg.* **57**(6):687–692.

Hassan, A.N., L.R. Beck, and S. Dister. 1998a. Prediction of villages at risk for filariasis transmission in the Nile Delta using remote sensing and geographic information system technologies. *J. Egypt. Soc. Parasitol.* **28**(1):75–87.

Hassan, A.N., S. Dister, and L. Beck. 1998b. Spatial analysis of lymphatic filariasis distribution in the Nile Delta in relation to some environmental variables using geographic information system technology. *J. Egypt. Soc. Parasitol.* **28**(1):119–131.

Hlavka, C., and E. Sheffner. 1988. *The California cooperative remote sensing project: Final report.* NASA Tech. Memo 100073. NASA Ames Research Center, Moffett Field, CA. 94 pp.

Hay, S.I., M.J. Packer, and D.J. Rogers. 1997. The impact of remote sensing on the study and control of invertebrate intermediate hosts and vectors for disease. *Int. J. Remote Sens.* **18**(14):2899–2930.

Hay, S., C. Tucker, D. Rogers, and M. Packer. 1996. Remotely sensed surrogates of meteorological data for the study of the distribution and abundance of arthropod vectors of disease. *Ann. Trop. Med. Parasit.* **90**(1):1–19.

Hayes, R., E. Maxwell, C. Mitchell, and T. Woodzick. 1985. Detection, identification, and classification of mosquito larval habitats using remote sensing scanners in earth-orbiting satellites. *Bulletin World Health Org.* **63**:361–374.

Hutchinson, C. 1982. Techniques for combining Landsat and ancillary data for digital classification improvement. *Photogram. Engin. Rem. Sensing* **48**:123–130.

Markos, B.G. 1951. Distribution and abundance of mosquito larvae and pupae in rice fields in Stanislaus County, California. *J. Nat. Malar. Soc.* **10**:233–247.

Markos, B.G., and E.J. Sherman. 1957. Additional studies on the distribution of mosquito larvae and pupae within a rice field check. *Mosq. News* **17**:40–43.

Martin, R.D. Jr., and J.L. Heilman. 1986. Spectral reflectance patterns of flooded rice. *Photogram. Engin. Rem. Sensing* **52**(12):1885–1890.

National Aeronautics and Space Administration (NASA). 1988. *A project plan for vector-borne disease predictive modeling (Project Di-Mod).* NASA Ames Research Center, Moffett Field, CA, unpublished.

Patel, N.K., N. Ravi, R.R. Navalgund, R.N. Dash, K.C. Das, and S. Patnaik. 1991. Estimation of rice yield using IRS-1A digital data in coastal tract of Orissa. *Int. J. Rem. Sensing* **12**(11):2259–2266.

Strahler, A. 1980. The use of prior probabilities in maximum likelihood classification of remotely sensed data. *Rem. Sensing Environ.* **10**:135–163.

Swain, P., J. Richards, and T. Lee. 1985. Multisource data analysis in remote sensing and geographic information processing. *Proc. Symp. Machine Process. of Remotely Sensed Data*. LARS, Purdue University, West Lafayette, IN, pp. 211–218.

Wall, S., C. Brown, and R. Thomas. 1980. *Remote sensing of rice and related crops — A review of pertinent research by the University of California.* Remote Sensing Research Program, Series 22, Issue 25. University of California, Berkeley. 22pp.

Washino, R. 1980. Mosquitoes—a by-product of rice culture. *Calif. Agric.* **34**:11–12.

Washino, R., M. Pitcairn, and E. Rejmánková. 1987. *Remote sensing for identification of mosquito larval habitats.* Mosquito Control Research: Annual Report. Div. Agriculture and Natural Resources, University of California, Davis, unpublished.

Washino, R., M. Pitcairn, and E. Rejmánková. 1988. *Remote sensing mosquito prediction project: Final report.* NASA Grant NAGW-81096, unpublished.

Welsh, J., J. Olson, M. Yates, A. Benton, Jr., and R. Baker. 1989. Conceptual model for the use of aerial color-infrared photography by mosquito control districts as a survey technique for *Psorophora columbiae* oviposition habitats in Texas ricelands. *J. Amer. Mosq. Contr. Assoc.* **5**:369–373.

Wood, B.L., L.R. Beck, R.K. Washino, K.A. Hibbard, and J. Salute. 1992. Estimating high mosquito-producing rice fields using spectral and spatial data. *Int. J. Rem. Sensing* **13**(15):2813–2826.

Wood, B.L, L.R. Beck, R.K. Washino, S.M. Palchick, and P.D. Sebesta. 1991a. Spectral and spatial characterization of rice field mosquito habitat. *Int. J. Rem. Sensing* **12**(3):621–626.

Wood, B., R. Washino, L. Beck, K. Hibbard, M. Pitcairn, D. Roberts, E. Rejmánková, J. Paris, C. Hacker, J. Salute, P. Sebesta, and L. Legters. 1991b. Distinguishing high and low anopheline-producing rice fields using remote sensing and GIS technologies. *Prev. Vet. Med.* **11**:277–288.